Mechanisms by which Cytoplasmic Calcium Wave Propagation and Alternans Are Generated in Cardiac Atrial Myocytes Lacking T-Tubules—Insights from a Simulation Study

Qince Li,[†] Stephen C. O'Neill,[‡] Tao Tao,[†] Yatong Li,[‡] David Eisner,[‡] and Henggui Zhang[†§*]

[†]Biological Physics Group, School of Physics and Astronomy and [‡]Unit of Cardiac Physiology, School of Biomedicine, The University of Manchester, Manchester, United Kingdom; and [§]School of Computer Science and Technology, Harbin Institute of Technology, Harbin, China

ABSTRACT This study investigated the mechanisms underlying the propagation of cytoplasmic calcium waves and the genesis of systolic Ca^{2+} alternans in cardiac myocytes lacking transverse tubules (t-tubules). These correspond to atrial cells of either small mammals or large mammals that have lost their t-tubules due to disease-induced structural remodeling (e.g., atrial fibrillation). A mathematical model was developed for a cluster of ryanodine receptors distributed on the cross section of a cell that was divided into 13 elements with a spatial resolution of 2 μm. Due to the absence of t-tubules, L-type Ca^{2+} channels were only located in the peripheral elements close to the cell-membrane surface and produced Ca^{2+} signals that propagated toward central elements by triggering successive Ca^{2+}-induced Ca^{2+} release (CICR) via Ca^{2+} diffusion between adjacent elements. Under control conditions, the Ca^{2+} signals did not fully propagate to the central region of the cell. However, with modulation of several factors responsible for Ca^{2+} handling, such as the L-type Ca^{2+} channels (Ca^{2+} influx), SERCA pumps (sarcoplasmic reticulum (SR) Ca^{2+} uptake), and ryanodine receptors (SR Ca^{2+} release), Ca^{2+} wave propagation to the center of the cell could occur. These simulation results are consistent with previous experimental data from atrial cells of small mammals. The model further reveals that spatially functional heterogeneity in Ca^{2+} diffusion within the cell produced a steep relationship between the SR Ca^{2+} content and the cytoplasmic Ca^{2+} concentration. This played an important role in the genesis of Ca^{2+} alternans that were more obvious in central than in peripheral elements. Possible association between the occurrence of Ca^{2+} alternans and the model parameters of Ca^{2+} handling was comprehensively explored in a wide range of one- and two-parameter spaces. In addition, the model revealed a spontaneous second Ca^{2+} release in response to a single voltage stimulus pulse with SR Ca^{2+} overloading and augmented Ca^{2+} influx. This study provides what to our knowledge are new insights into the genesis of Ca^{2+} alternans and spontaneous second Ca^{2+} release in cardiac myocytes that lack t-tubules.

INTRODUCTION

Ca^{2+} plays a crucial role in cardiac electrical activity, which triggers mechanical contraction of the cell. Systolic $[Ca^{2+}]_i$ alternans (1,2) can produce alternans in action-potential duration, which may predispose to atrial or ventricular fibrillations (3–6). Previous experimental and simulation studies have revealed that a steep relationship between systolic $[Ca^{2+}]_i$ transient and sarcoplasmic reticulum (SR) Ca^{2+} content can produce fluctuation in the SR Ca^{2+} content. This in turn is responsible for generating $[Ca^{2+}]_i$ alternans in ventricular myocytes with transverse (t)-tubules (2,7,8).

However, the mechanisms underlying Ca^{2+} wave propagation and $[Ca^{2+}]_i$ alternans in cardiac myocytes lacking t-tubules are still unclear. In small mammals, a key structural difference between atrial and ventricular myocytes is that atrial cells lack t-tubules (9). In ventricular cells, or those from the atria of large mammals, t-tubules may be lost during remodeling processes associated with some diseases, such as atrial fibrillation (10) or heart failure (11–13). In myocytes devoid of t-tubules, voltage-operated calcium channels (VOCCs) are only located on the peripheral cell membrane (9), and therefore, Ca^{2+} signals produced by depolarization of cell-membrane potential first appear at the subsarcolemmal region and then move to the central region of the cell by triggering successive calcium-induced calcium release (CICR) (14,15). It is unclear whether the dramatic difference in Ca^{2+} handling between cells with and those without t-tubules has a different impact on Ca^{2+} wave propagation and therefore on the genesis of $[Ca^{2+}]_i$ alternans.

In the work presented here, we attempted to develop a biophysically detailed computer model for Ca^{2+} release and Ca^{2+} wave propagation in cardiac myocytes lacking t-tubules. The model was used to investigate possible mechanisms underlying the emergence of Ca^{2+} alternans in cardiac cells.

METHODS

Mathematical model of Ca^{2+} wave propagation in atrial myocytes

The model was based on equations describing the dynamics of intracellular-Ca^{2+} handling for a generic cardiac myocyte that were implemented by Kurata et al. (16) for sinoatrial node cells. The Kurata et al. model was later modified by Tao et al. (8) to simulate intracellular Ca^{2+}-wave propagation in ventricular cells. In the study presented here, we further modified the Tao et al. equations (8) to simulate intracellular Ca^{2+}-wave propagation in atrial myocytes that lack t-tubules. In this atrial model, the cross section of a cell

Submitted August 2, 2011, and accepted for publication March 2, 2012.

*Correspondence: henggui.zhang@manchester.ac.uk

Editor: Godfrey Smith.

0006-3495/12/04/1471/12 $2.00

doi: 10.1016/j.bpj.2012.03.007

(with a diameter of 26 μm) is divided into 13 elements with a spatial resolution of 2 μm (Fig. 1 *A i*), which is close to the distance between neighboring Ca^{2+}-release sites seen in the central and peripheral regions of an atrial cell (9). VOCCs are localized at the two peripheral units close to the cell membrane surface. The Ca^{2+} cycling scheme in the peripheral elements is shown in Fig. 1 *A ii*. In the central elements, Ca^{2+} cycling is similar to that of the peripheral units but without those elements present in the surface membrane, e.g., VOCCs. These elements are coupled by Ca^{2+} diffusion between neighboring cytoplasmic spaces adjacent to junctional and nonjunctional ryanodine receptors (RyRs) and between neighboring network SR spaces (Fig. 1 *A i*). The diffusion parameter, D, used in the model produces a Ca^{2+}-wave conduction velocity of ~230 μm s^{-1}, which is consistent with experimental data (10) and previous models (17,18). Details of Ca^{2+} handling, diffusion equations, and parameters are given in the Supporting Material.

Stimulation protocol and simulated intracellular Ca^{2+}-wave propagation

In simulations, $[Ca^{2+}]_i$ transients were produced by a series of voltage-clamp pulses (1 Hz), as used in previous experimental studies (7). In each of the voltage-clamp pulses, cell membrane potential was clamped from a holding potential of −40 mV to a test potential of 0 mV for 100 ms.

In response to each voltage-clamp pulse, the model produced intracellular Ca^{2+} diffusion and subsequent Ca^{2+}-wave propagation (Fig. 1 *B i*). The simulated time traces of $[Ca^{2+}]_i$ and $[Ca^{2+}]_{SR}$ in both the peripheral (*black arrow*) and central (*red arrow*) regions (Fig. 1 *B i*) are shown in Fig. 1, *B ii* and *B iii*, respectively. Under control conditions, on each voltage-clamp pulse, Ca^{2+} influx via VOCCs triggered CICR at the peripheral units, resulting in large $[Ca^{2+}]_i$ transients in these regions. These localized $[Ca^{2+}]_i$ transients diffused inward toward the central region, provoking successive CICR that led to Ca^{2+}-wave propagation. However, the inward Ca^{2+} wave did not fully propagate to the center (Fig. 1 *B i*), because the gradually decreasing $[Ca^{2+}]_i$ transient amplitude (Fig. 1 *B ii*) provided an insufficient trigger to generate further CICR, causing the wave to terminate. Consequently, the $[Ca^{2+}]_i$ transients (Fig. 1 *B ii*) and the SR Ca^{2+} release (Fig. 1 *B iii*) were large in the periphery of the cell but small in the central region, leading to a spatially heterogeneous distribution of $[Ca^{2+}]_i$ transients and Ca^{2+} wave propagation (Fig. 1 *B i*). These simulation results matched experimental observations in rat (15,19), guinea-pig (20), and cat (4) atrial myocytes that lack t-tubules.

Model validation

For the purpose of validation, a series of simulations was performed and compared to previous experimental observations from small mammal atrial myocytes that lack t-tubules. These simulations included the effects of sustaining the intracellular Ca^{2+} waves through increasing Ca^{2+} influx by elevating the extracellular Ca^{2+} concentration ($[Ca^{2+}]_o$, (Fig. S1)), increasing the RyR sensitivity by decreasing the threshold of RyR for CICR (Fig. S2), and elevating the SR content by pausing pacing for 10 s while increasing SERCA Ca^{2+} uptake (P_{up} increased by 75%) to allow SR Ca^{2+} content accumulation (Fig. S3). In the model, it was shown that increases in the Ca^{2+} influx, the RyR sensitivity, or the SR content helped to sustain full Ca^{2+}-wave propagation from the periphery to the center of the cell, producing a more homogeneous $[Ca^{2+}]_i$ transient across the cell. These simulation results were similar to experimental observations (Fig. S1, Fig. S2, and Fig. S3).

RESULTS

Effect of increasing Ca^{2+} influx

An increase in Ca^{2+} influx via elevating $[Ca^{2+}]_o$ has been shown to help facilitate full Ca^{2+}-wave propagation toward the center region and to reduce the $[Ca^{2+}]_i$ spatial heterogeneity in atrial cells (15). This experimental observation was reproduced by the model (Fig. S1). In this study, we investigated the effect of an augmented Ca^{2+} influx from a different approach, i.e., by increasing the maximum channel

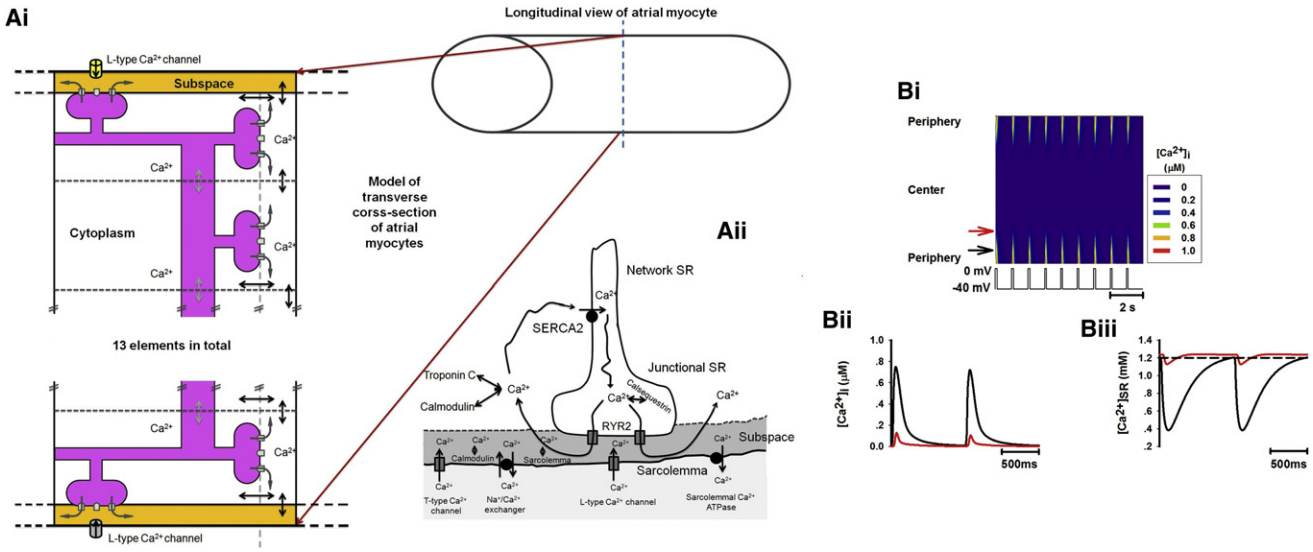

FIGURE 1 Schematic model of Ca^{2+} handling in atrial myocytes lacking t-tubules, and simulated Ca^{2+}-wave propagation under control condition. (*A i*) A cluster of coupled RyRs on a transverse cross section of an atrial myocyte. The cross section is divided into 13 coupled elements, each of which represents a cluster of RyRs. (*A ii*) Schematic model of calcium cycling for the peripheral elements of the cluster shown in *A i*. (*B i*) Line-scan image of cytoplasmic $[Ca^{2+}]_i$ transients throughout the atrial myocyte. The voltage trace below marks each of the stimulus pulses (similar in subsequent figures). (*B ii* and *B iii*) Time traces of cytoplasmic $[Ca^{2+}]_i$ transient (*B ii*) and SR Ca^{2+} content (*B iii*) corresponding to different regions of the cell (*black*, peripheral region; *red*, central region; see online color figure).

conductance of the VOCCs (g_{CaL}). Results are shown in Fig. 2. Fig. 2 *A* shows a line scan of the $[Ca^{2+}]_i$ transient across the cell, with an expanded plot of the line-scan image for the time period marked by the horizontal bracket and asterisk (*inset A*). In the simulation, the cell was paced under control conditions for several beats before g_{CaL} was increased by a factor of 5. Upon the increase of g_{CaL}, full propagation of the Ca^{2+} wave to the center was seen (Fig. 2 *A*). Fig. 2, *B* and *C*, shows the time courses of the $[Ca^{2+}]_i$ transient and the SR Ca^{2+} content ($[Ca^{2+}]_{SR}$) recorded from sites near the periphery (*black*; see online color figure) and in the central region (*red*; see online color figure) for control (Fig. 2 *B*) and increased-g_{CaL} (Fig. 2 *C*) conditions. The $[Ca^{2+}]_i$ transient was heterogeneous across the cell under the control condition (Fig. 2 *B*) but more homogeneous when full inward Ca^{2+}-wave propagation was evoked by increasing g_{CaL} (Fig. 2 *C*). Insets *B* and *C* (Fig. 2, *B* and *C*, respectively) clearly illustrate that there is a time delay in the $[Ca^{2+}]_i$ and $[Ca^{2+}]_{SR}$ transients between the peripheral and central regions of the cell, indicating Ca^{2+}-wave propagation from the peripheral toward the central region of the cell that triggered successive Ca^{2+} release, rather than a synchronized Ca^{2+} release across the cell.

The generation of a full Ca^{2+} wave upon increasing g_{CaL} is attributable to a large $[Ca^{2+}]_i$ transient in the peripheral region (Fig. 2, *B* and *C*, *upper*), rather than to altered SR Ca^{2+} content (Fig. 2, *B* and *C*, *lower*). An increased Ca^{2+} influx produced a large $[Ca^{2+}]_i$ transient in the peripheral region, thus promoting enhanced centerward Ca^{2+} diffusion, which activated successive CICR in elements toward the central region.

Effect of increasing RyR sensitivity

Fig. 3 shows the impact of enhancing the RyR sensitivity by reducing the threshold of RyR for CICR (K_{rel}). In this simulation, the cell was initially stimulated under control conditions for 2 s before K_{rel} was reduced by 10% (Fig. 3, *A i* and *B i*) and 60% (Fig. 3, *A ii* and *B ii*). The corresponding line-scan images of cytoplasmic Ca^{2+} are shown in Fig. 3, *A i* and *A ii*, respectively. $[Ca^{2+}]_i$ transients and SR Ca^{2+} contents, recorded from both peripheral and central regions, are shown in Fig. 3, *B i* and *B ii*, respectively, which are compared to those obtained under control conditions (Fig. 3 *B*). When K_{rel} was reduced by 10%, a complete Ca^{2+} wave spreading toward the interior region of the cell was established temporarily (Fig. 3 *A i*). However, the amplitude of the $[Ca^{2+}]_i$ transient recorded from either the peripheral or the central region was smaller (Fig. 3 *B i*, *upper*) than that seen in Fig. S2, where RyR sensitivity

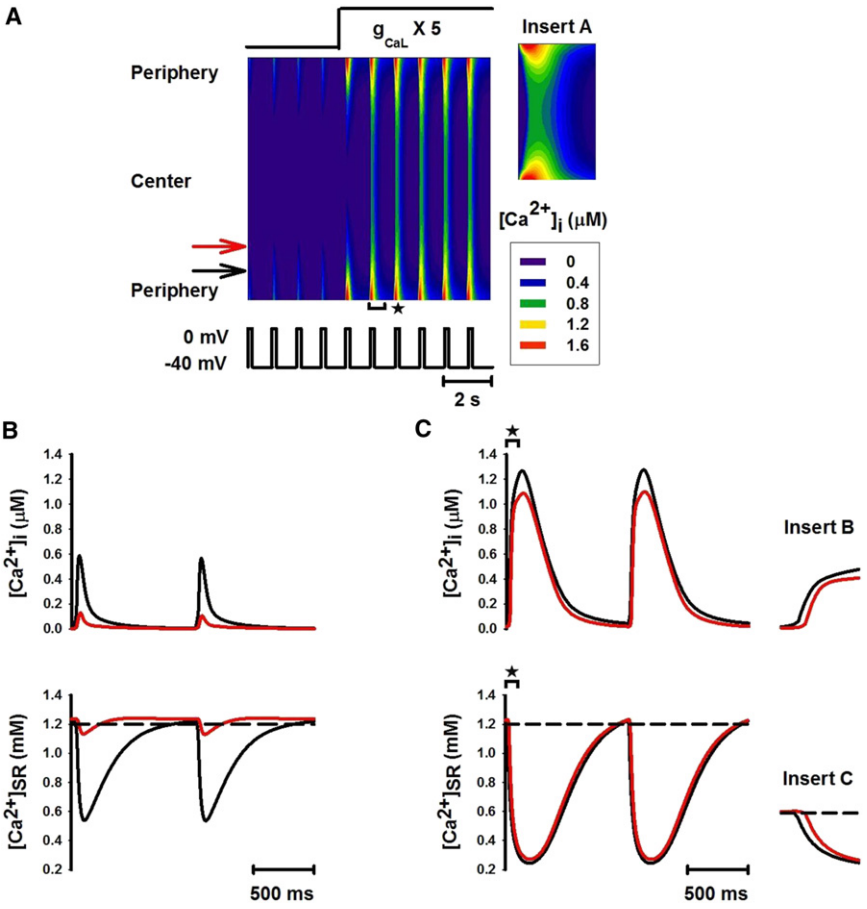

FIGURE 2 Fully propagated Ca^{2+} wave and homogeneous $[Ca^{2+}]_i$ transients induced by increasing g_{CaL}. (*A*) Line-scan image of cytoplasmic $[Ca^{2+}]_i$ transients. g_{CaL} was increased to five times its control value after the first four pulses. (*Inset A*) Expanded plot from the line-scan image for the time period marked by the bracket with asterisk in *A* (similar in subsequent figures). (*B* and *C*) Traces of $[Ca^{2+}]_i$ transients (*upper*) and Ca^{2+} concentration in the SR space (*lower*) recorded from peripheral (*black*; see online color figure) and central (*red*; see online color figure) regions of the cell before (*B*) and after (*C*) increasing the L-type calcium current. (*Insets B* and *C*) Expanded plots of $[Ca^{2+}]_i$ and $[Ca^{2+}]_{SR}$ traces for the time periods marked by the horizontal brackets with asterisks in *C*.

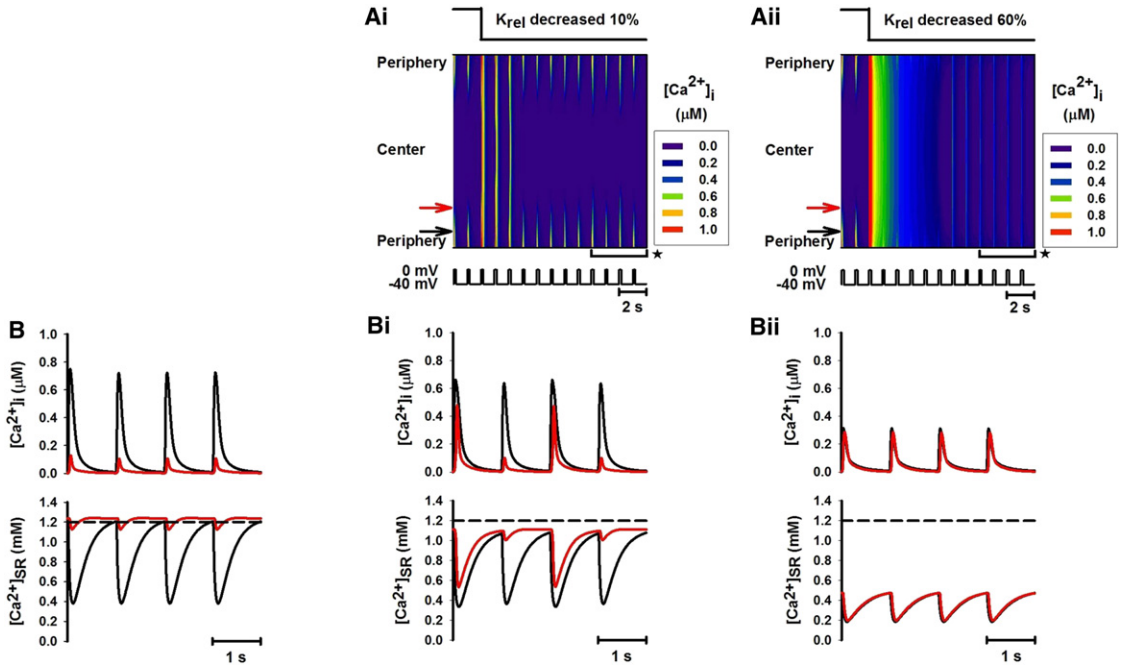

FIGURE 3 Effect of increasing the sensitivity of RyRs by decreasing K_{rel} by 10% and 60%. (*A i* and *A ii*) Line-scan images of spatial patterns of $[Ca^{2+}]_i$ transients produced by decreasing K_{rel} by 10% and 60%, respectively. (*B*, *B i*, and *B ii*) Traces of $[Ca^{2+}]_i$ transients (*upper*) and Ca^{2+} concentration in the SR space (*lower*) recorded from peripheral (*black*; see online color figure) and central (*red*; see online color figure) regions of the cell before (*B*) and after (*B i* and *B ii*) increasing the sensitivity of RyRs. *B i* and *B ii* are the time traces recorded during the time period marked by the horizontal brackets with asterisks shown in *A i* and *A ii*.

was increased while SR content was maintained. This was attributed to a reduced level of $[Ca^{2+}]_{SR}$ (Fig. 3 *B i*, *lower*) compared to control and Fig. S2 conditions, as more Ca^{2+} in the SR was released to the cytoplasmic space. Due to the reduced SR content, propagation of the Ca^{2+} wave toward the center of the cell was unstable, leading to alternans between a complete Ca^{2+} wave and an incomplete Ca^{2+} wave after a few pulses (Fig. 3, *A i* and *B i*). This produced $[Ca^{2+}]_i$ alternans in both peripheral and central regions (Fig. 3 *B i*; *upper*), which were associated with alternating SR Ca^{2+} content (Fig. 3 *B i*, *lower*). However, a stable complete Ca^{2+} wave was observed when K_{rel} was reduced by >60% (Fig. 3 *A ii*), with even smaller amplitude of $[Ca^{2+}]_i$ across the cell due to even greater reduction of SR Ca^{2+} content (Fig. 3 *B ii*).

Effect of increased SR content

The effects of increased SR Ca^{2+} content on Ca^{2+}-wave propagation were investigated in two ways. In one approach, the SR Ca^{2+} content was increased by pausing voltage-clamp pulse for 10 s after the initial 3 s of stimulations. In the other, the SR content was increased by increasing the SR Ca^{2+} uptake rate (P_{up}) by 70%. The results are shown in Fig. 4.

Fig. 4 *A i* shows a line-scan image of the effects of pausing stimulation. The corresponding time traces for the $[Ca^{2+}]_i$ transient and the SR Ca^{2+} contents recorded from the peripheral and central regions before (Fig. 4 *B*) and after (Fig. 4 *B i*) pausing stimulation are shown. Stopping the voltage-clamp pulse for 10 s increased SR Ca^{2+} content (Fig. 4 *B i*, *lower*), leading to a period of complete Ca^{2+} wave propagation into the center of the cell (Fig. 4 *A i*), which was followed by alternating complete and incomplete Ca^{2+} waves (Fig. 4, *A i* and *B i*). This produced $[Ca^{2+}]_i$ alternans in both peripheral and central regions (Fig. 4 *B i*, *upper*). Insets A and B (Fig. 4, *B i*, *upper* and *lower*, respectively) demonstrate the time delays in the $[Ca^{2+}]_i$ and $[Ca^{2+}]_{SR}$ transients between the peripheral and central regions of the cell, illustrating that Ca^{2+} transients were not invoked homogeneously across the cell.

Fig. 4 *A ii* is a line-scan image of cytoplasmic Ca^{2+} after increasing P_{up}, and Fig. 4 *B ii* shows the corresponding time series for $[Ca^{2+}]_i$ and $[Ca^{2+}]_{SR}$ recorded from the peripheral and central regions. It is clear that the SR Ca^{2+} content was gradually elevated in both the peripheral and central regions by enhancing the SR Ca^{2+} uptake (Fig. 4 *B ii*). During the first 3-s voltage-clamp pulse after increasing P_{up}, the elevation of the SR Ca^{2+} content in the central region was small. Thus, increasing SR Ca^{2+} uptake expedited the decline of local $[Ca^{2+}]_i$ and hindered the inward Ca^{2+} wave propagation (Fig. 4 *A ii*). However, 5 s after elevating P_{up}, a stable complete Ca^{2+} wave was observed (Fig. 4 *A ii*) when the SR Ca^{2+} content was significantly elevated in both central and peripheral regions (Fig. 4 *B ii*, *lower*). Insets C and D (Fig. 4 *B ii*, *upper* and *lower*, respectively) represent the time delay in the $[Ca^{2+}]_i$ and $[Ca^{2+}]_{SR}$ transients between

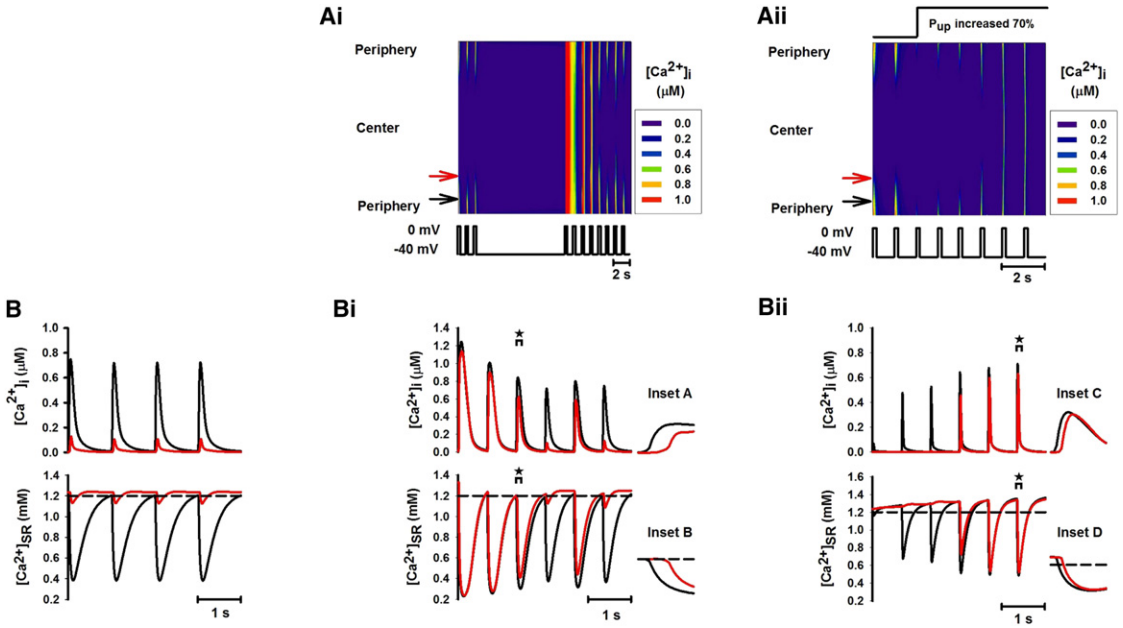

FIGURE 4 Effects of elevated SR Ca^{2+} content on Ca^{2+}-wave propagation by pausing pacing for 10 s when $[Ca^{2+}]_o$ was increased from 1 mM to 10 mM and by increasing SR uptake rate P_{up} by 70%. (*A i* and *A ii*) Line-scan images of spatial patterns of $[Ca^{2+}]_i$ transients produced by pausing voltage-clamp pulse and increasing P_{up}, respectively. (*B*, *B i*, and *B ii*) Traces of $[Ca^{2+}]_i$ (*upper*) and $[Ca^{2+}]_{SR}$ (*lower*) recorded from peripheral (*black*; see online color figure) and central (*red*; see online color figure) regions of the cell before (*B*) and after (*B i* and *B ii*) elevating the SR Ca^{2+} content. (*Insets A–D*) Expanded plots of the time traces for the time periods marked by the brackets with asterisks shown in *B i* and *B ii*.

the peripheral and central regions of the cell, indicating that the Ca^{2+} wave was first initiated in the periphery and then conducted toward the center of the cell.

Effect of partial inhibition of SERCA pump

In simulations, two different approaches were implemented to reduce the SERCA pump activity. In one approach, SERCA pump rate (P_{up}) was decreased by 10%. The results are shown in Fig. 5. After P_{up} was decreased, the reduced SR Ca^{2+} uptake enhanced Ca^{2+}-wave propagation (Fig. 5 *A i*) when the SR Ca^{2+} content was comparable to that under control conditions (Fig. 5, *B* and *B i*, *lower*). However, in a subsequent voltage-clamp pulse, the SR Ca^{2+} contents in both the peripheral and central regions declined due to defective SERCA pump activity. This led to a smaller Ca^{2+} release in the peripheral region and a diminished Ca^{2+} wave in the central region (Fig. 5, *A i* and *B i*), and produced $[Ca^{2+}]_i$ transient alternans (Fig. 5 *B i*, *upper*).

In the other approach, the SERCA pump activity was inhibited by increasing the threshold of SERCA Ca^{2+} uptake (K_{up}) by 20% (Fig. 5 *A ii*). Meanwhile the SERCA pump rate (P_{up}) was increased by 50% such that the SR Ca^{2+} content was maintained close to that in control condition. An enhanced Ca^{2+}-wave propagation was established, as shown in Fig. 5 *A ii*. In this case, $[Ca^{2+}]_i$ transients at the peripheral sites remained almost unchanged (Fig. 5, *B* and *B ii*). However, the amplitude of $[Ca^{2+}]_i$ transients was greatly enhanced in the interior region of the cell (Fig. 5 *B ii*, *upper*), leading to full Ca^{2+}-wave propagation, though the SR Ca^{2+} content was comparable to that in control condition (Fig. 5, *B* and *B ii*, *lower*). This was attributed to the fact that a partial inhibition of SERCA activity while the SR Ca^{2+} content was maintained resulted in more diffusion of Ca^{2+} throughout the cell. In addition to the increased $[Ca^{2+}]_i$ transients in the central region, the Ca^{2+} signal displayed alternans (Fig. 5 *B ii*, *upper*) that was more obvious in the central region than in the periphery (Fig. 5 *A ii*, *insets A and B*). These Ca^{2+} alternans arose because the Ca^{2+} release propagated toward the interior. The resulting large Ca^{2+} release depleted the SR content in the central region, which did not fully recover by the next voltage-clamp pulse, resulting in a reduced Ca^{2+} release. In this way, an alternating large-small pattern of $[Ca^{2+}]_i$ transients was produced.

Exploring the mechanisms for Ca^{2+} alternans

Further simulations were performed to explore possible mechanisms by which Ca^{2+} alternans in cardiac myocytes without t-tubules could be generated in response to a linear change in the parameters associated with various aspects of Ca^{2+} handling.

Role of Ca^{2+} diffusion

Fig. 6 *A* shows the effect of a linear increase of the time constant of the Ca^{2+} diffusion (τ) on generation of $[Ca^{2+}]_i$ alternans. When τ was varied from 100% to 130% of its

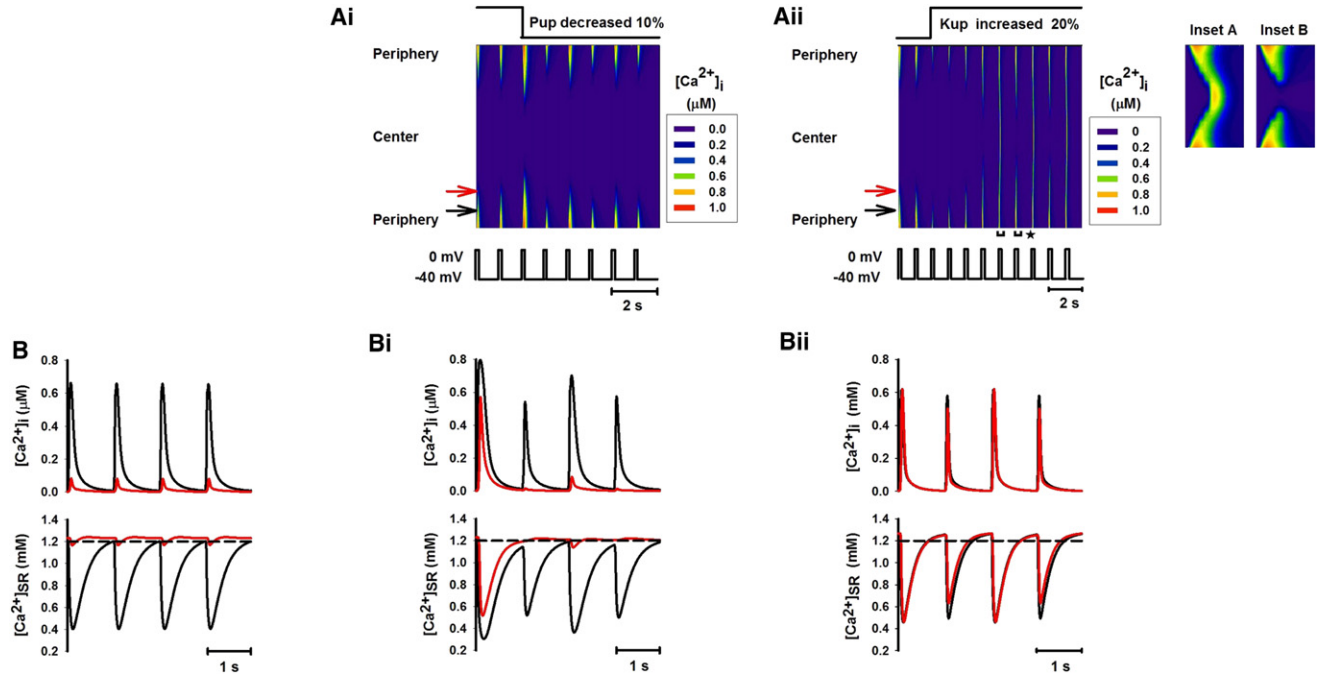

FIGURE 5 Ca^{2+} propagation with partial inhibition of SR Ca^{2+} uptake by decreasing the SR uptake rate (P_{up}) by 10% and increasing the SERCA uptake threshold (K_{up}) by 20%. In the latter case, P_{up} was increased by 50% to keep SR Ca^{2+} content comparable to that of the control condition. (*A i* and *A ii*) Line-scan images of spatial patterns of $[Ca^{2+}]_i$ transients produced by decreasing P_{up} and increasing K_{rel}, respectively. (*Insets A* and *B*) Expanded plots from the line-scan image in *A ii* for the time periods marked by the horizontal brackets with asterisks (*left*, *Inset A*; *right*, *Inset B*). (*B*, *B i*, and *B ii*) Time traces of $[Ca^{2+}]_i$ (*upper*) and $[Ca^{2+}]_{SR}$ (*lower*) recorded from peripheral (*black*; see online color figure) and central (*red*; see online color figure) regions of the cell before (*B*) and after (*B i* and *B ii*) inhibiting SERCA activity.

control value, various patterns of Ca^{2+} alternans were observed (Fig. 6 *A*, *upper*). Transition to such variant $[Ca^{2+}]_i$ alternans was via a bifurcation process (Fig. 6 *A*, *lower*), which occurred when τ was 115% of its control value, with each large Ca^{2+} transient being followed first by four (Fig. 6 *A i*), then two (Fig. 6 *A ii*), then one (Fig. 6 *A iii*) small one. This suggested that a more complicated pattern of $[Ca^{2+}]_i$ alternans than that typically observed (1:1 $[Ca^{2+}]_i$ alternans) was possible. Note that such a complicated pattern of alternans has been observed experimentally in the electrical activity of the heart with period doubling and tripling and even more complicated 1:n patterns generated by a cascade effect of the bifurcation process (21).

We further examined the effect of Ca^{2+} diffusion on genesis of $[Ca^{2+}]_i$ alternans by removing the Ca^{2+} diffusion in the cell. In the absence of Ca^{2+} diffusion (i.e., the model was considered as a single unit), partial inhibition of SERCA activity by increasing K_{up} by 20% or even by 40% did not produce Ca^{2+} alternans. This indicated an important role of Ca^{2+} diffusion in generating $[Ca^{2+}]_i$ alternans.

Such an important role of Ca^{2+} diffusion in generating alternans can be understood by analyzing the dependence of the systolic $[Ca^{2+}]_i$ amplitude on the SR Ca^{2+} content, which was derived by correlating the SR Ca^{2+} content to the systolic $[Ca^{2+}]_i$ amplitude during refilling of the SR from the empty state. Results shown in Fig. 6 *B* were obtained at the control condition. In this case, diffusion dramatically increased the steepness of this dependence (from n = 4.0 in the absence of diffusion to 25.3 for diffusion).

It has been suggested previously that increased dependence of Ca^{2+} release on SR Ca^{2+} content increases the probability of alternans occurring (2,7). In ventricular myocytes, it was shown (7) that reducing the activation of $I_{Ca,L}$ channels—thus producing a small Ca^{2+} signal for triggering CICR of RyR channels—increased the steepness of dependence of Ca^{2+} release on SR Ca^{2+} content, leading to genesis of $[Ca^{2+}]_i$ alternans. In atrial myocytes devoid of t-tubules, the $I_{Ca,L}$ channels are only located in the peripheral region. In the interior region of the cell, it is Ca^{2+} diffusion that provides a Ca^{2+} signal that triggers CICR of RyR channels. As the Ca^{2+} signal for triggering CICR via such Ca^{2+} diffusion is small, one would also expect a steep dependence of Ca^{2+} release on SR Ca^{2+} content.

In the model with Ca^{2+} diffusion, the effect of partial inhibition of SERCA activity (increasing K_{up} by 20%) on the steepness of the $[Ca^{2+}]_i$ dependence on the SR Ca^{2+} content is shown in Fig. 6 *C*. Increasing K_{up} shifted the dependence curve leftward (i.e., toward smaller SR Ca^{2+} content region) compared with that under the control condition, indicating a more sensitive dependence of the systolic

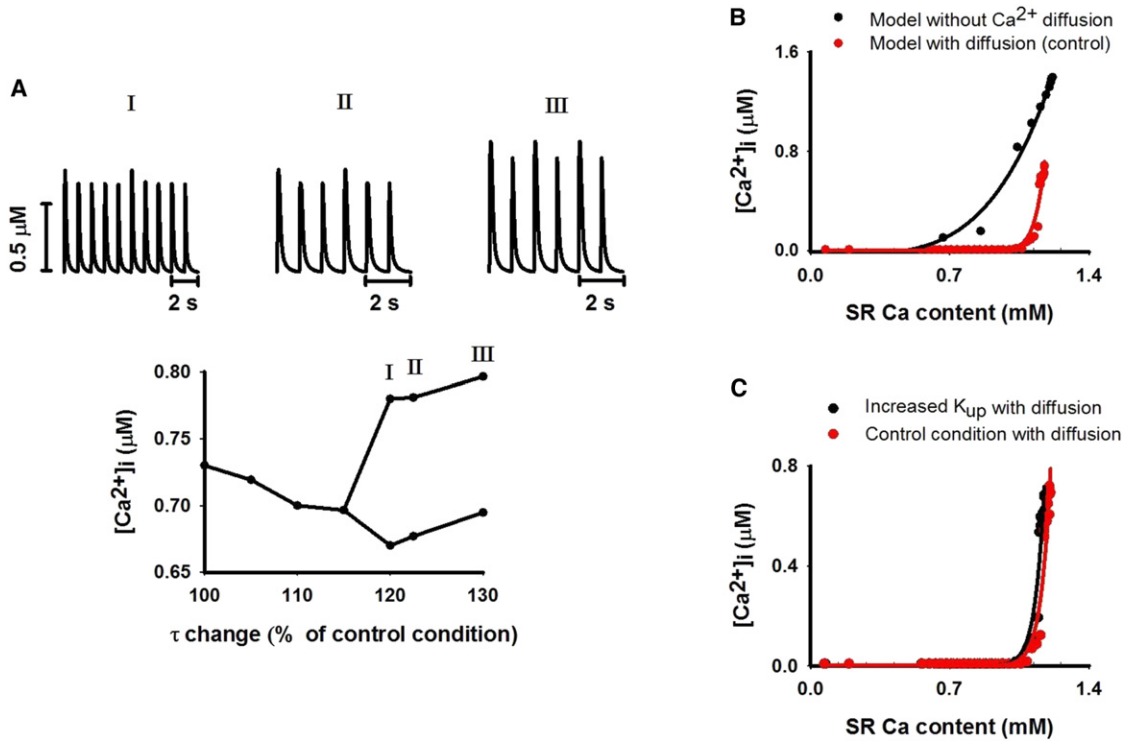

FIGURE 6 Role of Ca^{2+} diffusion in generating $[Ca^{2+}]_i$ alternans. (*A*, *upper*) Various patterns of $[Ca^{2+}]_i$ alternans generated by varying the Ca^{2+} diffusion constant (τ). (*A*, *lower*) Systolic $[Ca^{2+}]_i$ amplitudes as a function of τ increased over the range 100% to 130% of its control value. A bifurcation process occurred, leading to $[Ca^{2+}]_i$ alternans with complicated patterns of 1:4 (*I*), 1:2 (*II*), and 1:1 (*III*) alternans. (*B*) Relationship between systolic $[Ca^{2+}]_i$ amplitude and SR Ca^{2+} content with (*red*; see online color figure) and without (*black*; see online color figure) Ca^{2+} diffusion. The solid lines were generated by using the formula for curve fitting (amplitude of systolic $[Ca^{2+}]_i = a + b \times [\text{SR } Ca^{2+} \text{ content}]^n$). n = 4.0 for the model without Ca^{2+} diffusion, and n = 25.3 for the model with Ca^{2+} diffusion. (*C*) Relationship between systolic $[Ca^{2+}]_i$ amplitude and SR calcium content in a model with Ca^{2+} diffusion, but with (*black dots*; see online color figure) (n = 25.3) or without (*red dots*; see online color figure) (n = 25.3) partial inhibition of SERCA pump activity.

$[Ca^{2+}]_i$ amplitude on the SR content, which enabled the genesis of $[Ca^{2+}]_i$ alternans (Fig. 5 *A ii*).

Role of Ca^{2+} influx

The role of increased Ca^{2+} influx in generating $[Ca^{2+}]_i$ alternans was investigated by systematically increasing g_{CaL}. When g_{CaL} was increased over the range 100%–500% of its control value, a cascade of bifurcations occurred, leading to $[Ca^{2+}]_i$ alternans with various patterns (Fig. 7 *A i*). In all cases, $[Ca^{2+}]_i$ alternans was more dramatic in the central region than in the peripheral region (Fig. 7, *A ii* and *A iii*). In the range 120%–150% of g_{CaL}, a very small $[Ca^{2+}]_i$ transient amplitude in the central region associated with 1:2 alternans (Fig. 7, *A i I* and *A iv*) indicated a partial propagation of a Ca^{2+} wave into the central region for every two out of three Ca^{2+} waves, each of which resulted in a marked spatial gradient in $[Ca^{2+}]_i$ amplitude across the cell. In the range 150–170% of g_{CaL}, $[Ca^{2+}]_i$ alternans disappeared (Fig. 7, *A i II* and *A iv*), but it reappeared when g_{CaL} was further increased to 200%–400% of its control value (Fig. 7, *A i III*, *A i IV*, and *A iv*). In the latter case, although the amplitude of the $[Ca^{2+}]_i$ transient alternated from beat to beat, its spatial gradient across the cell was reduced, as the amplitude of the $[Ca^{2+}]_i$ transient in the central region was close to that in the peripheral region (Fig. 7 *A iv*). $[Ca^{2+}]_i$ alternans disappeared when g_{CaL} was increased to >450% (Fig. 7, *A ii* and *A iii*).

Role of RyR sensitivity

The role of increased sensitivity of RyR to CICR in generating $[Ca^{2+}]_i$ alternans was investigated by reducing K_{rel} from 100% to 60% of its control value. With decreasing K_{rel}, a cascade of bifurcations occurred, leading to $[Ca^{2+}]_i$ alternans with various patterns (Fig. 7 *B i*). Similar to the case of increasing $g_{Ca,L}$, $[Ca^{2+}]_i$ alternans was more significant in the central region (Fig. 7, *B ii* and *B iii*). When K_{rel} was reduced to 90% of its control value, $[Ca^{2+}]_i$ alternans began with a 1:1 pattern (Fig. 7, *B i I* and *B iv*). It became more complicated when K_{rel} was reduced to 85%–55% (Fig. 7, *B i II* and *B iv*). Further reducing K_{rel} to <40% caused $[Ca^{2+}]_i$ alternans to disappear (Fig. 7, *B i III* and *B iv*). In the latter case, small $[Ca^{2+}]_i$ transients were seen in both the peripheral and central regions, leading to a decreased spatial gradient of the $[Ca^{2+}]_i$ transient in the cell. It was due to the fact that the increased sensitivity of RyRs in nonjunctional regions enabled them to be more

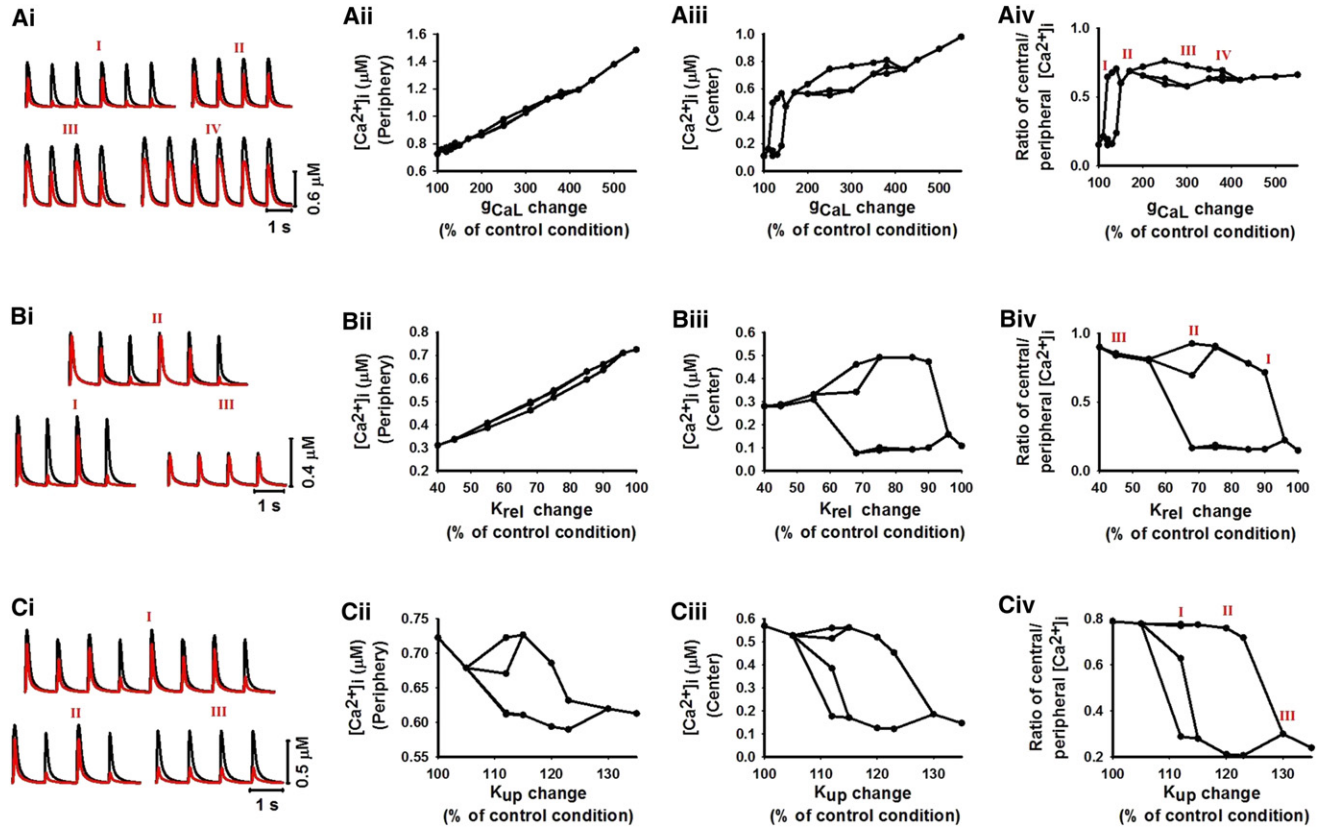

FIGURE 7 Roles of altered Ca^{2+} influx (*A*, *i–iv*), sensitivity of RyR (*B*, *i–iv*), and SERCA pump activity (*C*, *i–iv*) in generating $[Ca^{2+}]_i$ alternans. The bifurcation diagram was drawn by plotting multiple peak values of the Ca^{2+} transient for a given $g_{Ca,L}$, K_{rel}, or K_{up}. (*A i*, *B i*, and *C i*) Various profiles of Ca^{2+} transients recorded in peripheral (*black*; see online color figure) and central (*red*; see online color figure) regions of the cell. Profiles were generated by a cascade of bifurcation processes with a linear increase of $g_{Ca,L}$ (*A i*) and K_{up} (*C i*) and a decrease of K_{rel} (*B i*). (*A ii*, *B ii*, and *C ii*) Amplitude of systolic $[Ca^{2+}]_i$ transient against $g_{Ca,L}$ (*A ii*), K_{rel} (*B ii*), and K_{up} (*C ii*) in the peripheral region of the cell. (*A iii*, *B iii*, and *C iii*) Amplitude of systolic $[Ca^{2+}]_i$ transient versus $g_{Ca,L}$ (*A iii*), K_{rel} (*B iii*), and K_{up} (*C iii*) in the central region of the cell. (*A iv*, *B iv*, and *C iv*) Ca^{2+} gradient measured as the ratio between the central and peripheral Ca^{2+} amplitudes with a linear increase of $g_{Ca,L}$ (*A iv*) and K_{rel} (*B iv*) and a decrease of K_{up} (*C iv*). Small ratios represent a large gradient; ratios approaching 1 imply more homogeneous Ca^{2+} distribution in the cell.

easily triggered for CICR at a lower level of the SR content, producing small but homogeneous $[Ca^{2+}]_i$ transients across the cell (Fig. 7 *B iv*).

Role of the SERCA pump

The role of a defective SERCA pump in generating $[Ca^{2+}]_i$ alternans was investigated by modulating the half-maximal cytoplasmic $[Ca^{2+}]_i$ for SERCA Ca^{2+} uptake (K_{up}). When K_{up} was increased from 100% to 140% of its control value, a cascade of bifurcations was triggered, leading to Ca^{2+} alternans with different patterns (Fig. 7 *C i*). When K_{up} was increased by 10%, $[Ca^{2+}]_i$ alternans had a complicated pattern (Fig. 7, *C i I* and *C iv*), but it transited into 1:1 alternans when K_{up} was increased by 20% (Fig. 7, *C i II* and *C iv*). When K_{up} was increased by >30%, $[Ca^{2+}]_i$ alternans disappeared (Fig. 7, *C i III* and *C iv*). In all cases, decreased SR uptake due to increased K_{up} resulted in a low level of SR Ca^{2+} content and, consequently, reduced $[Ca^{2+}]_i$ transient amplitude (Fig. 7, *C ii* and *C iii*). However, the spatial gradient in $[Ca^{2+}]_i$ transient across the cell was augmented by the defective SR uptake, which gradually depleted the SR content (Fig. 7 *C iv*).

Further simulations were performed to explore theoretically the genesis of $[Ca^{2+}]_i$ alternans in a 2D parameter space, mimicking combined modulations of two different properties of Ca^{2+} handling, which may occur in some disease conditions, such as heart failure, where the sensitivity of RyRs is enhanced, whereas the SERCA activity is significantly reduced (22). Detailed results are shown in in the Supporting Material.

Spontaneous Ca^{2+} release

Overloading the SR Ca^{2+} content may produce spontaneous Ca^{2+} release from the SR. Fig. 8 shows recorded time traces of $[Ca^{2+}]_i$ (Fig. 8 *A i*), $[Ca^{2+}]_{SR}$ (Fig. 8 *A ii*), Ca^{2+}-Na^+ exchange current (I_{NCX}; Fig. 8 *A iii*), and I_{CaL} (Fig. 8 *A iv*) recorded from the cell under the condition of increased Ca^{2+} influx (g_{CaL} increased to 370%) and SERCA pump activity (P_{up} increased to 150%). With dramatic increases in both the

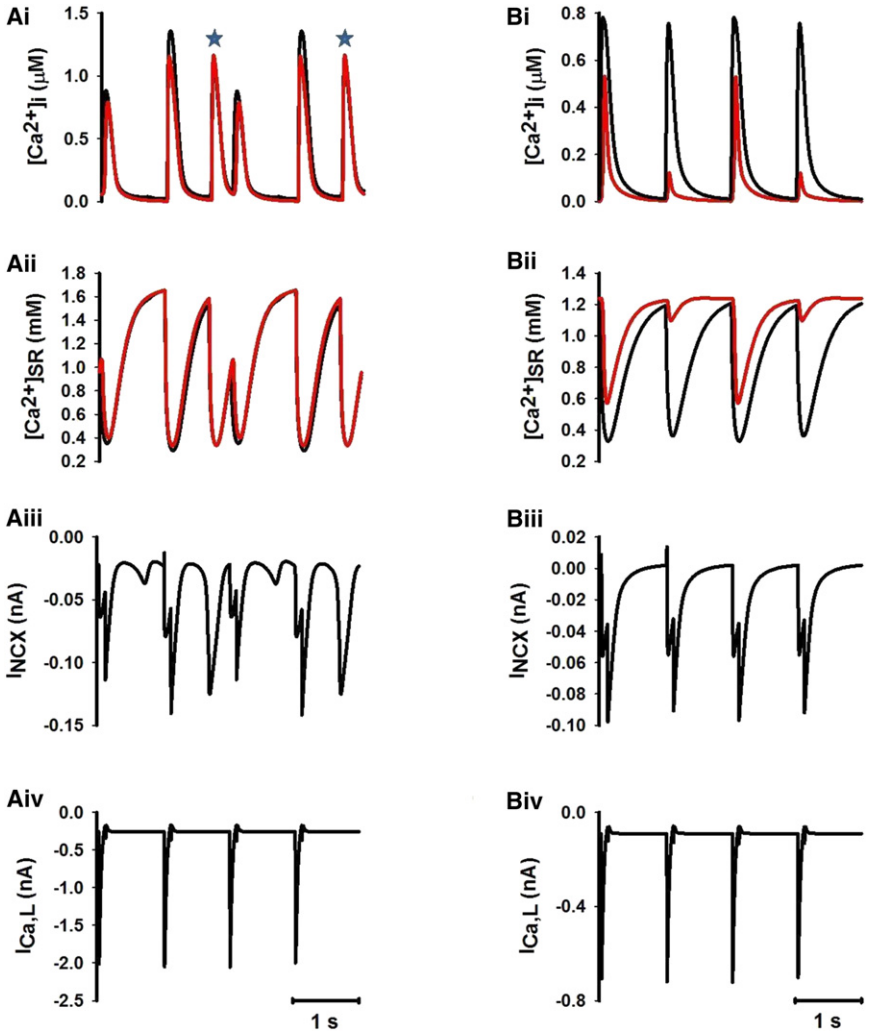

FIGURE 8 (*A i–A iv*) Time traces of $[Ca^{2+}]_i$ (*A i*), SR Ca^{2+} content (*A ii*), Na^+-Ca^{2+} exchange current (I_{NCX}) (*A iii*), and $I_{Ca,L}$ (*A iv*) under the condition of SR Ca^{2+} overload (P_{up} increased to 150%) and increased Ca^{2+} influx ($g_{Ca,L}$ increased to 370%) for peripheral (*black*; see online color figure) and central (*red*; see online color figure) regions of the cell. Irregular $[Ca^{2+}]_i$ transients were produced, as were spontaneous secondary SR Ca^{2+} releases in response to a single voltage-clamp pulse (*asterisks*). (*B i–B iv*) Time traces of $[Ca^{2+}]_i$ (*B i*), SR Ca^{2+} content (*B ii*), Na^+-Ca^{2+} exchange current (I_{NCX}) (*B iii*), and $I_{Ca,L}$ (*B iv*) under the condition of increasing $g_{Ca,L}$ by 30% of its control value. Highly sensitive dependence of $[Ca^{2+}]_i$ transient on SR Ca^{2+} content led to genesis of $[Ca^{2+}]_i$ alternans.

Ca^{2+} influx and the SR uptake efficiency, an irregular pattern of $[Ca^{2+}]_i$ transient was observed in response to a series of stimuli. A most interesting observation was the spontaneous second SR Ca^{2+} releases in response to one stimulus (Fig. 8 *A i*, *asterisks*).

DISCUSSION

Summary of major findings

We have developed a mathematical model for Ca^{2+}-wave propagation in cardiac atrial myocytes that lack t-tubules, thereby representing atrial myocytes of small mammals, or atrial cells of larger mammals, that have lost t-tubules due to disease-induced structural remodeling. The developed model was validated by its ability to reproduce typical Ca^{2+}-wave propagation patterns of atrial myocytes without t-tubules. It was also validated by its ability to reproduce experimentally observed effects of modulations of various aspects of Ca^{2+} cycling, such as Ca^{2+} influx, SERCA pumps (SR Ca^{2+} uptake), and RyRs (SR Ca^{2+} release), on spatial distribution of Ca^{2+} transients (15). Using the model, we explored possible factors responsible for generating Ca^{2+} alternans in cardiac cells devoid of t-tubules. The major findings of this study are as follows. 1), The functional spatial heterogeneity in Ca^{2+} diffusion due to gradually decreased amplitudes of Ca^{2+} transients across the cell produced a steep relationship between the SR Ca^{2+} content and the cytoplasmic Ca^{2+} concentration. Together with Ca^{2+} wave propagation, this contributed to the genesis of Ca^{2+} alternans, which was more obvious in central than in peripheral elements. 2), Analyses on one-parameter space and two-parameter space (see Supporting Material) were performed to provide a theoretical exploration of possible associations between the occurrence of Ca^{2+} alternans and parameters related to calcium handling. In these analyses, either one or two parameters associated with Ca^{2+} handling were altered alone or together. 3), Under the condition of SR Ca^{2+} overload and augmented Ca^{2+} influx, the model predicted a spontaneous second Ca^{2+} release in response to

a single voltage-stimulus pulse. Spontaneous Ca^{2+} release may be responsible for ectopic activities, leading to atrial fibrillations (23). This study provides, for the first time to our knowledge, a biophysically detailed mathematical model of intracellular Ca^{2+} handling that underpins the mechanisms of Ca^{2+}-wave propagation in cardiac myocytes that lack t-tubules. It also offers what to our knowledge are new insights into the genesis of Ca^{2+} alternans and spontaneous Ca^{2+} release, both of which are proarrhythmic.

Mechanisms of incomplete Ca^{2+}-wave propagation in cardiac cells without t-tubules

It has been shown that in atrial myocytes without t-tubules, the Ca^{2+} signal is restricted to the junctional subsarcolemmal compartment (9,15) due to incomplete Ca^{2+}-wave propagation in the cell. It was hypothesized that this was due to the reduction in amplitude of Ca^{2+} transients from the peripheral to the central regions of the cell, leading to a gradual reduction in Ca^{2+} diffusion. Thus, moving toward the central region, the decreased Ca^{2+} signal produced smaller CICR and further reduced Ca^{2+} signals until CICR could not be induced in the central region of the cell. This led to an incomplete Ca^{2+} wave propagation (9). Our simulation results support this theory (Fig. 1). The model reproduced spatially inhomogeneous Ca^{2+} transients across the cell. With a gradual decrease in amplitude, Ca^{2+} diffusion becomes reduced from the peripheral region to the central region, leading to reduced CICR trigger at interior sites, which results in termination of the Ca^{2+} wave when the trigger is insufficient for further SR Ca^{2+} release at the interior region. However, modulations of Ca^{2+} handling that enhanced intracellular Ca^{2+} diffusion from the peripheral to the central region, such as increasing Ca^{2+} influx by increasing g_{CaL} (Fig. 2), increasing the sensitivity of RyRs by lowering the threshold of RyRs (Fig. 3), increasing the SR Ca^{2+} content (Fig. 4), or reducing the SERCA pump activity (Fig. 5), helped to establish a complete Ca^{2+} wave across the cell.

Mechanisms of Ca^{2+} alternans in cardiac cells devoid of t-tubules

Roles of Ca^{2+} diffusion

The results of Fig. 6 clearly indicate an important contribution of Ca^{2+} diffusion in generating Ca^{2+} alternans. In the model, upon partial inhibition of SERCA pump activity, 1:1 Ca^{2+} alternans was produced. However, with the same set of model parameters, no Ca^{2+} alternans was observed if the cell was treated as a single release element, or with t-tubules across the cell with VOCC channels being coupled with all RyR elements, i.e., no Ca^{2+} diffusion in the model. Further analysis revealed that Ca^{2+} diffusion altered the relationship between the SR Ca^{2+} load and the systolic Ca^{2+} concentration in cytoplasm by sharply increasing the steepness of this relationship (Fig. 6 *B*), enabling the genesis of Ca^{2+} alternans. In the model, the Ca^{2+} diffusion was induced by a spatially inhomogeneous distribution of Ca^{2+} transients across the cell due to the lack of t-tubules in the central region. This was fundamentally different from ventricular myocytes, where the existence of t-tubules inside cells was expected to produce a more simultaneous and homogeneous distribution of Ca^{2+} transients in the cross section of the cell.

Roles of Ca^{2+}-handling kinetics—insights from one-parameter analysis

Similar to previous modeling studies on ventricular cells with t-tubules (8), Ca^{2+} alternans can also be generated in cardiac myocytes absent of t-tubules by changing properties of Ca^{2+} cycling. Varying an individual parameter (Fig. 7) associated with Ca^{2+} influx (g_{CaL}), SR Ca^{2+} release (K_{rel}), and SR Ca^{2+} uptake (K_{up}) triggered a cascade bifurcation process, leading to complex patterns of Ca^{2+} alternans as a consequence of interactions between Ca^{2+} diffusion and altered Ca^{2+} cycling in individual elements. Such interactions produced a steep relationship between the SR Ca^{2+} content and cytoplasmic Ca^{2+} transients, resulting in a highly sensitive dependence of Ca^{2+} release on the SR content. This was illustrated in Fig. 8, *B*, *i–iv*, which plotted the time series of $[Ca^{2+}]_i$ (Fig. 8 *B i*), $[Ca^{2+}]_{SR}$ (Fig. 8 *B ii*), I_{NCX} (Fig. 8 *B iii*), and I_{CaL} (Fig. 8 *B iv*) when $[Ca^{2+}]_i$ alternans were produced by increasing g_{CaL} to 130% of its control value (Fig. 7 *A*). It was obvious that the SR Ca^{2+} load was slightly lower before a small Ca^{2+} release than before a large release (Fig. 8 *B ii*). Corresponding to a larger $[Ca^{2+}]_i$ transient, there was a greater removal of cytoplasmic Ca^{2+} by NCX current (Fig. 8 *B iii*), which led to incomplete refilling of the SR (Fig. 8 *B ii*), producing a smaller Ca^{2+} release (Fig. 8 *B ii*), minor Ca^{2+}-wave propagation, and Ca^{2+} efflux by the next stimulus. All of these effects enabled SR Ca^{2+} content to recover to the normal level, producing a large Ca^{2+} release on the next stimulus (7,8,24). During all of the $[Ca^{2+}]_i$ alternating processes, the amplitude of $I_{Ca,L}$ remained unchanged (Fig. 8 *B iv*). In some conditions, several cycles might be needed for the SR Ca^{2+} content to recover to a normal level after a large Ca^{2+} release, producing more complicated patterns ($1{:}n-1$, where $n > 1$) of Ca^{2+}-transient alternans.

Significance of the study

It has been observed that t-tubule networks are dense and well organized in ventricular myocytes, are absent or less organized in other types of cardiac cells, including atrial cells (3,19). However, recent studies have identified t-tubules in atrial myocytes from a number of species, including sheep (10,11), dog (25), and human (26). Further studies have also shown that t-tubules of atrial and ventricular cells may be

lost or disorganized by structural remodeling processes during chronic diseases (11,13). Loss of t-tubules of ventricular myocytes has been observed in a number of animal models of heart failure, as well as in human heart failure (27). Dramatic loss of t-tubules was also observed in atrial myocytes in a sheep model of heart failure (12) and in patients with persistent atrial fibrillation (10).

Thus, this study provides insight into the mechanisms underlying Ca^{2+}-wave propagation in cardiac myocytes, not only for atrial myocytes of small mammals that lack t-tubules but also for other cardiac myocytes (including ventricular myocytes) that lose t-tubules due to disease-induced structural remodeling. Experimental studies show that the loss of t-tubules in ventricular myocytes due to detubulation (9) is associated with desynchronized Ca^{2+} release across the cell, and Ca^{2+} wavelike propagation from the sarcolemma to the cell interior. In a similar way, loss of t-tubules in atrial myocytes during atrial fibrillation is also associated with spatially desynchronized Ca^{2+} release (10). All of these features observed in ventricular and atrial myocytes with loss of t-tubules were reproduced in the model.

In this study, we also investigated the mechanisms underlying the genesis of Ca^{2+} alternans and spontaneous RyR Ca^{2+} release, both of which are proarrhythmic, in cardiac cells devoid of t-tubules. It was shown that the absence of t-tubules promoted the genesis of Ca^{2+} alternans due to Ca^{2+} diffusion consequent to heterogeneous distribution of Ca^{2+} transients across the cell. Ca^{2+} alternans were generated for conditions under which no Ca^{2+} alternans would be observed if t-tubules were present. This may provide a partial explanation to the increased risk of arrhythmogenesis in cardiac tissues remodeled by chronic diseases such as heart failure and atrial fibrillation.

Limitations of the study

This model was based on the Kurate et al. (16) and Tao et al. (8) models and inherited the same limitations of that model, which have been discussed in detail in our previous study (8). The major limitation of this model was its use of one-dimensional RyR elements on the cross section of a cell, which is an idealized consideration of the cell. It therefore lacked the complex geometry of a whole cell, which imposes 3-dimensional structure and features complicated t-tubule networks and RyR arrangement. In simulations, the inositol-1,4,5-trisphosphate-receptor (IP_3R) was not incorporated into the model, because the contribution of IP_3R-mediated Ca^{2+} release to atrial $[Ca^{2+}]_i$ remains controversial and is limited under the basal condition (28). On the one hand, the lack of consideration of IP_3Rs in our model may be considered a potential limitation of this study. On the other hand, however, it makes clear the importance of Ca^{2+} diffusion and various factors of Ca^{2+} handling in the generation of Ca^{2+} waves and alternans in cardiac myocytes without t-tubules.

All of these limitations are now being addressed for future versions of the model. However, they do not alter our conclusions about the mechanisms that underlie the initiation and propagation of Ca^{2+} waves in cardiac myocytes lacking t-tubules or the genesis of Ca^{2+} alternans in this type of cell.

SUPPORTING MATERIAL

Details of Ca^{2+} handling, diffusion equations, equation parameters, results of two-parameter space analysis, eight figures, and references are available at http://www.biophysj.org/biophysj/supplemental/S0006-3495(12)00289-5.

This work was supported by project grants from the Engineering and Physical Science Research Council UK (EP/I029826/1; EP/J00958X/1) and the National Science Foundation China (61179009). Q.L. was supported by an Overseas Research Scholarship from The University of Manchester.

REFERENCES

1. Chudin, E., J. Goldhaber, …, B. Kogan. 1999. Intracellular Ca^{2+} dynamics and the stability of ventricular tachycardia. *Biophys. J.* 77:2930–2941.
2. Eisner, D. A., H. S. Choi, …, A. W. Trafford. 2000. Integrative analysis of calcium cycling in cardiac muscle. *Circ. Res.* 87:1087–1094.
3. Blatter, L. A., J. Kockskämper, …, S. L. Lipsius. 2003. Local calcium gradients during excitation-contraction coupling and alternans in atrial myocytes. *J. Physiol.* 546:19–31.
4. Kockskämper, J., and L. A. Blatter. 2002. Subcellular Ca^{2+} alternans represents a novel mechanism for the generation of arrhythmogenic Ca^{2+} waves in cat atrial myocytes. *J. Physiol.* 545:65–79.
5. Narayan, S. M., F. Bode, …, M. R. Franz. 2002. Alternans of atrial action potentials during atrial flutter as a precursor to atrial fibrillation. *Circulation.* 106:1968–1973.
6. Pruvot, E. J., R. P. Katra, …, K. R. Laurita. 2004. Role of calcium cycling versus restitution in the mechanism of repolarization alternans. *Circ. Res.* 94:1083–1090.
7. Díaz, M. E., S. C. O'Neill, and D. A. Eisner. 2004. Sarcoplasmic reticulum calcium content fluctuation is the key to cardiac alternans. *Circ. Res.* 94:650–656.
8. Tao, T., S. C. O'Neill, …, H. Zhang. 2008. Alternans of cardiac calcium cycling in a cluster of ryanodine receptors: a simulation study. *Am. J. Physiol. Heart Circ. Physiol.* 295:H595–H609.
9. Brette, F., and C. Orchard. 2003. T-tubule function in mammalian cardiac myocytes. *Circ. Res.* 92:1182–1192.
10. Lenaerts, I., V. Bito, …, R. Willems. 2009. Ultrastructural and functional remodeling of the coupling between Ca^{2+} influx and sarcoplasmic reticulum Ca^{2+} release in right atrial myocytes from experimental persistent atrial fibrillation. *Circ. Res.* 105:876–885.
11. Balijepalli, R. C., A. J. Lokuta, …, T. J. Kamp. 2003. Depletion of T-tubules and specific subcellular changes in sarcolemmal proteins in tachycardia-induced heart failure. *Cardiovasc. Res.* 59:67–77.
12. Dibb, K. M., J. D. Clarke, …, A. W. Trafford. 2009. Characterization of an extensive transverse tubular network in sheep atrial myocytes and its depletion in heart failure. *Circ. Heart Fail.* 2:482–489.
13. Louch, W. E., H. K. Mørk, …, O. M. Sejersted. 2006. T-tubule disorganization and reduced synchrony of Ca^{2+} release in murine cardiomyocytes following myocardial infarction. *J. Physiol.* 574:519–533.
14. Carl, S. L., K. Felix, …, D. G. Ferguson. 1995. Immunolocalization of sarcolemmal dihydropyridine receptor and sarcoplasmic reticular triadin and ryanodine receptor in rabbit ventricle and atrium. *J. Cell Biol.* 129:673–682.

15. Mackenzie, L., H. L. Roderick, …, M. D. Bootman. 2004. The spatial pattern of atrial cardiomyocyte calcium signalling modulates contraction. *J. Cell Sci.* 117:6327–6337.

16. Kurata, Y., I. Hisatome, …, T. Shibamoto. 2002. Dynamical description of sinoatrial node pacemaking: improved mathematical model for primary pacemaker cell. *Am. J. Physiol. Heart Circ. Physiol.* 283:H2074–H2101.

17. Backx, P. H., P. P. de Tombe, …, H. E. ter Keurs. 1989. A model of propagating calcium-induced calcium release mediated by calcium diffusion. *J. Gen. Physiol.* 93:963–977.

18. Langer, G. A., and A. Peskoff. 1996. Calcium concentration and movement in the diadic cleft space of the cardiac ventricular cell. *Biophys. J.* 70:1169–1182.

19. Woo, S. H., L. Cleemann, and M. Morad. 2002. Ca^{2+} current-gated focal and local Ca^{2+} release in rat atrial myocytes: evidence from rapid 2-D confocal imaging. *J. Physiol.* 543:439–453.

20. Berlin, J. R. 1995. Spatiotemporal changes of Ca^{2+} during electrically evoked contractions in atrial and ventricular cells. *Am. J. Physiol.* 269:H1165–H1170.

21. Ritzenberg, A. L., D. R. Adam, and R. J. Cohen. 1984. Period multupling-evidence for nonlinear behaviour of the canine heart. *Nature.* 307:159–161.

22. Yamamoto, T., M. Yano, …, M. Matsuzaki. 1999. Abnormal Ca^{2+} release from cardiac sarcoplasmic reticulum in tachycardia-induced heart failure. *Cardiovasc. Res.* 44:146–155.

23. Hove-Madsen, L., A. Llach, …, J. Cinca. 2004. Atrial fibrillation is associated with increased spontaneous calcium release from the sarcoplasmic reticulum in human atrial myocytes. *Circulation.* 110:1358–1363.

24. Shiferaw, Y., and A. Karma. 2006. Turing instability mediated by voltage and calcium diffusion in paced cardiac cells. *Proc. Natl. Acad. Sci. USA.* 103:5670–5675.

25. Dolber, P. C., R. P. Bauman, …, J. C. Greenfield, Jr. 1994. Regional changes in myocyte structure in model of canine right atrial hypertrophy. *Am. J. Physiol.* 267:H1279–H1287.

26. Richards, M. A., J. D. Clarke, …, K. M. Dibb. 2011. Transverse tubules are a common feature in large mammalian atrial myocytes including human. *Am. J. Physiol. Heart Circ. Physiol.* 301:H1996–H2005.

27. Lyon, A. R., K. T. MacLeod, …, J. Gorelik. 2009. Loss of T-tubules and other changes to surface topography in ventricular myocytes from failing human and rat heart. *Proc. Natl. Acad. Sci. USA.* 106:6854–6859.

28. Li, X., A. V. Zima, …, J. Chen. 2005. Endothelin-1-induced arrhythmogenic Ca^{2+} signaling is abolished in atrial myocytes of inositol-1,4,5-trisphosphate(IP_3)-receptor type 2-deficient mice. *Circ. Res.* 96:1274–1281.